NeuroImage 172 (2018) 575–585

Contents lists available at ScienceDirect

NeuroImage

journal homepage: www.elsevier.com/locate/neuroimage

Envelope analysis links oscillatory and arrhythmic EEG activities to two types of neuronal synchronization

Javier Díaz [a,*], Alejandro Bassi [a], Alex Coolen [b], Ennio A. Vivaldi [a], Juan-Carlos Letelier [c]

[a] Laboratorio de Sueño y Cronobiología, Programa de Fisiología y Biofísica, Instituto de Ciencias Biomédicas (ICBM), Facultad de Medicina, Universidad de Chile, Santiago, Chile
[b] Groningen Institute of Evolutionary Life Sciences, University of Groningen, The Netherlands
[c] Facultad de Ciencias, Universidad de Chile, Chile

A B S T R A C T

Traditionally, EEG is understood as originating from the synchronous activation of neuronal populations that generate rhythmic oscillations in specific frequency bands. Recently, new neuronal dynamics regimes have been identified (e.g. neuronal avalanches) characterized by irregular or arrhythmic activity. In addition, it is starting to be acknowledged that broadband properties of EEG spectrum (following a $1/f$ law) are tightly linked to brain function. Nevertheless, there is still no theoretical framework accommodating the coexistence of these two EEG phenomenologies: rhythmic/narrowband and arrhythmic/broadband. To address this problem, we present a new framework for EEG analysis based on the relation between the Gaussianity and the envelope of a given signal. EEG Gaussianity is a relevant assessment because if EEG emerges from the superposition of uncorrelated sources, it should exhibit properties of a Gaussian process, otherwise, as in the case of neural synchronization, deviations from Gaussianity should be observed. We use analytical results demonstrating that the coefficient of variation of the envelope (*CVE*) of Gaussian noise (or any of its filtered sub-bands) is the constant $\sqrt{\frac{4}{\pi}-1} \approx 0.523$, thus enabling *CVE* to be a useful metric to assess EEG Gaussianity. Furthermore, a new and highly informative analysis space (*envelope characterization space*) is generated by combining the *CVE* and the envelope average amplitude. We use this space to analyze rat EEG recordings during sleep-wake cycles. Our results show that delta, theta and sigma bands approach Gaussianity at the lowest EEG amplitudes while exhibiting significant deviations at high EEG amplitudes. Deviations to *low-CVE* appeared prominently during REM sleep, associated with theta rhythm, a regime consistent with the dynamics shown by the synchronization of weakly coupled oscillators. On the other hand, deviations to *high-CVE*, appearing mostly during NREM sleep associated with EEG phasic activity and high-amplitude Gaussian waves, can be interpreted as the arrhythmic superposition of transient neural synchronization events. These two different manifestations of neural synchrony (*low-CVE/high-CVE*) explain the well-known spectral differences between REM and NREM sleep, while also illuminating the origin of the EEG $1/f$ spectrum.

Introduction

In the early days of electroencephalograms (EEG), Adrian and Matthews proposed neural synchrony as the origin of Berger's rhythm (Adrian and Matthews, 1934). Nowadays, it is widely accepted that synchrony is one of the main mechanisms underlying EEG (Buzsáki et al., 2012) as well as being a crucial process in neural dynamics (Singer and Gray, 1995; Varela et al., 2001; von der Malsburg, 2000). The cornerstone of Adrian and Matthews' EEG seminal interpretation is that alpha rhythms appear when neurons *beat synchronously*, and that non synchronous neuronal activity abolishes prominent rhythms, causing instead an irregular activity of lower amplitude. This notion relating synchrony with EEG changes, in both amplitude and morphology, seems so obvious that it is accepted almost without effort. Nevertheless, the neuronal dynamics underlying these processes are still poorly understood (Nunez and Srinivasan, 2006). Thus, despite the very well-known relations between EEG patterns and brain states (Stern and Engel, 2005), a comprehensive theory accounting for all these patterns is not yet available.

Formal analysis shows that the amplitude for EEG arising from fully synchronized neuronal oscillators should be proportional to N (number of oscillators involved), while the expected amplitude for the EEG arising from an asynchronous neuronal population should instead be proportional to $\sqrt{N}$ (Elul, 1971; Díaz et al., 2007). Nevertheless, real world EEG signals present more complex possible scenarios than complete synchronization or full desynchronization. Synchronous neuronal populations may only encompass an unknown fraction of the total number of neurons contributing to EEG (Elul, 1971), and synchronized populations could be dynamically modulated with varying coupling constants (Breakspear et al., 2010; Schmidt et al., 2015). However, it is common to associate observable EEG amplitude fluctuations with neural synchrony

* Corresponding author.
E-mail address: javdiaz@uchile.cl (J. Díaz).

https://doi.org/10.1016/j.neuroimage.2018.01.063
Received 13 October 2017; Accepted 25 January 2018
Available online 2 February 2018

fluctuations. For example sleep EEG is traditionaly considered a *synchronized state*, while wake EEG is considered a *desynchronized state* (Steriade et al., 1990; Harris and Thiele, 2011). Moreover, due to modern ideas about neural plasticity (hebbian mechanisms, metaplasticity, and structural plasticity), EEG generation is seen as the result of the interplay of transient neural assemblies whose activities are network controlled by dynamically changing synaptic weights (Buzsáki, 2010; Buzsáki et al., 2012).

Alongside these mainstream ideas, alternative views concerning the origin of EEG appeared early in EEG research. Koiti Motokawa challenged Adrian's hypothesis about alpha rhythm origin (Motokawa and Mita, 1942), suggesting the superposition of *uncorrelated* oscillators explained alpha wave irregular patterns. Motokawa's paper was written in German during WWII and published in a Japanese journal making it difficult to track (Rao and Edwards, 2008). Similar results stressing the random component of alpha rhythms continued to resurface in the next decades (Sato, 1957; Saunders, 1963). A related statistical viewpoint can be found in the work of Elul who described the *Gaussian behaviour* of EEG as generated by the summation of independent oscillators in accordance with the central limit theorem (Elul, 1969). Other studies have focused on the arrhythmic nature of EEG, related to the characteristic $1/f$ -noise spectrum found in neural signals (Linkenkaer-Hansen et al., 2001; Freeman, 2006; He et al., 2010). More recently Biyu He has argued about the necessity to have a common theoretical framework to understand the interactions between rhythms and scale-free EEG activities (He, 2014). Another arrhythmic-related phenomenon is *neuronal avalanches* which correspond to a recently recognized class of neuronal dynamics (Beggs and Plenz, 2004) whose relation with scale-free activity is yet to be determined (He, 2014). Thus, even as the EEG nears its 100th anniversary, there are open questions at the very core of EEG research highlighted in a recent review entitled "Where does the EEG come from and what does it mean?" (Cohen, 2017).

In a previous report, we introduced an analysis of the envelope of neuronal signals that refuted the simple model linking synchrony with high amplitude oscillations. We showed that a purportedly good example of neuronal synchrony —the prominent oscillations observable in the olfactory epithelium of some vertebrates— could be better explained as the superposition of asynchronous neuronal activity (Díaz et al., 2007). In our results, the coefficient of variation of the envelope (*CVE*) of that neuronal wave was close to the fingerprint of randomness $\sqrt{\frac{4}{\pi}-1}$. We also predicted, considering two synchrony models (Matthews et al., 1991; Strogatz, 2000), that a neuronal wave originating from synchronous oscillators should exhibit a significantly lower *CVE*. Furthermore, we found the *CVE* is highly correlated with relevant aspects of signal morphology and can be used as a practical feature extraction method for neural signals and other bio-signals (Díaz et al., 2014).

Here, starting from rat EEG, we introduce a neural dynamic model that joins synchronous oscillations and arrhythmic EEG activities in a common framework using the envelope of EEG signals.

Methods

Animals and surgery. Experiments were performed in 7 Sprague-Dawley male rats (250-300 g) where at least 3 × 24 hour continuous recordings were done per rat, totaling 35 recording days. In each rat, subdural EEG and EMG electrodes were inserted under ketamine anesthesia surgical details in (Castro-Faúndez et al., 2016).

EEG and EMG recordings. Three days after surgery rats were placed in a 30 × 30 × 25 [cm] cage suspended within an 80 × 80 x 80 [cm] acoustically-isolated and temperature controlled (C) recording chamber under an artificial 12:12 light:dark cycle with lights-on (500 Lux) from 07:00 to 19:00 local time. Electrophysiological signals were amplified (2000 × for EEG and 5000 × for EMG), digitized (at 12 bits, 250 Hz per channel) and streamed to digital storage for off-line analysis. All data analysis, simulations and data visualization procedures were done using the *R* language (https://www.R-project.org/).

Data Analysis: Signal path, envelope construction and envelope-based calculations. As this work analyzes EEG based on signal envelopes, it is important to detail the mathematical steps applied to raw EEG signals (S). Each EEG trace, already divided in 24 h segments in phase with the Zeitgeber (starting at 7:00 AM), was digitally filtered to obtain its delta (δ: 0.5–4 Hz), theta (θ: 4-10 Hz) and sigma (σ: 11-16 Hz) bands using IIR fourth order Butterworth bandpass filters implemented in the *R* language (signal package – http://r-forge.r-project.org/projects/signal/). These three filtered signals ($S_f = S_\delta, S_\theta$ and S_σ) were cut into 24-s epochs (with 6000 samples per epoch). The Hilbert transform ($\mathscr{H}$) was then calculated for each epoch and for each band. The envelope of S_f was obtained using the standard result $env = \sqrt{S_f^2 + \mathscr{H}(S_f)^2}$. To avoid spurious results due to end effects, 2 s buffer segments at both ends were excised after envelope computation producing a 20 s epoch which was slided by 10 s, totaling 8640 epochs/day. The mean and standard deviation of env were calculated to obtain the coefficient of variation of the envelope ($CVE = sd(env)/mean(env)$) for delta, theta and sigma bands (CVE_δ, CVE_θ, CVE_σ).

Surrogate data models for Gaussianity. Vectors of length 6000 filled with Gaussian random values ($\sim N(0,1)$) were generated. As in real data, a 0.04 s sampling interval (equivalent to 250 Hz sampling rate) was assumed. These artificial 24-s epochs were filtered for delta, theta and sigma bands as indicated for the experimental data, and the envelope for these epochs was also obtained. At this point, the first and last 2 s (500 points from each end) were removed to eliminate end effects caused by digital filtering and envelope computation. For these trimmed 20-s epochs, CVE_δ, CVE_θ and CVE_σ were calculated for 10^6 epochs. Then, the probability density functions (PDF), as well as the cumulative density functions (CDF) were calculated and the 0.005 and 0.995 quantiles were determined to define the lower and upper limits of the 99% confidence interval for testing the H_0 hypothesis: EEG epoch resembles filtered white Gaussian noise. As EEG epochs have non-flat and dynamically changing power spectra we also explored the use of Fourier transform phase randomization (FTPR) epoch surrogates, as describes in (Galka, 2000). To obtain a PDF from FTPR epochs we used 116 phase randomized instances of 8640 epochs corresponding to a single day (equal to 1002240 epochs).

Expert WAKE/SLEEP cycle states scoring. The raw EEG data segmented into 10-s epochs was classified by a human scorer into Wake, NREM and REM states according to well-established rules for rat EEGs (Robert et al., 1999).

EMG activity processing. EMG signals were filtered (between 70 and 90 Hz) and cut into 20 s epochs (10 s overlap). For each epoch its RMS value was calculated producing a vector (with 8640 elements) representing the full 24 h cycle. To compare data from different rats, the RMS vector was normalized to $mean = 0$ and $sd = 1$.

Multitaper spectrogram. Time-frequency analysis was applied to EEG signals, divided in 20-s epochs and 10 s overlapping, according to (Prerau et al., 2016) using the *dpss* function in the *multitaper R* package with the following parameters: time-bandwidth = 10 and number of tapers = 20 (yielding a frequency resolution 0f 0.5 Hz). Frequencies higher than 20 Hz were discarded and the resulting spectral power, excluding the 2% minimal and maximal outliers, was log scaled and color coded (dark blue < cyan < orange < dark red).

Envelope characterization space (scatterplots and density maps). This phase space involves the *CVE* and the normalizaton ($mean = 0$ and $sd = 1$) of the logarithm of the envelope mean (as a parameter of EEG amplitude), both evaluated at the epoch level. This space was analyzed using scatterplots and density maps. These density maps were drawn by constructing 2D histograms on a 500 × 500 matrix. The rows and columns of these histograms were smoothed by 51-coefficient binomial kernels and visualized by using an alternating white/grey color palette that produces a contour-plot-like visualization of the histogram density.

CVE of artificial signals produced by pulse superposition. Artificial signals were constructed by the superposition of a variable number (in the

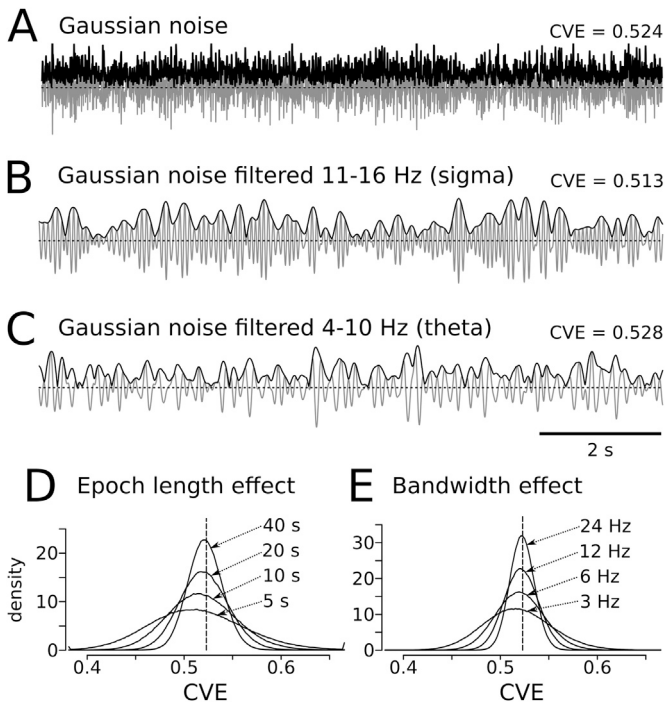

Fig. 1. Properties of the Coefficient of Variation of the Envelope (*CVE*) for Gaussian noise and derived bands. (A) A 10 s computer generated Gaussian noise (grey trace) and its corresponding envelope (black trace), obtained using the Hilbert Transform, in this case $CVE = 0.524$. (B) The same noise was bandpass filtered for the sigma (11-16 Hz) band (grey trace) and its envelope was calculated (black trace) producing a $CVE = 0.513$. (C) A similar procedure for the theta (4-10 Hz) band gives a $CVE = 0.528$. (D) Epoch length affects *CVE*. The *CVE* for 10^6 simulated 6Hz bandwidth filtered noise epochs of $5, 10, 20, 40$ s was calculated and distributions were determined. These empirical distributions are approximately Gaussian and their mode tends to 0.523 (as expected from theory). (E) Bandwidth affects *CVE*. The *CVE* for 10^6 simulated 20 s filtered noise epochs $3, 6, 12, 24$ Hz bandwidth was calculated and distributions were determined. These empirical distributions are also approximately Gaussian and their mode tends to 0.523 (dashed line).

sequence $(2^n)_{n=5}^{13}$) of Poisson distributed exponential decaying pulses ($p_i(t) = A_i \cdot e^{-\lambda t_i}$) with A_i randomly taken from an exponential distribution and λ_i uniformly distributed in the interval $[0.1 - 100]$ s^{-1}. The Fourier spectra of these signals were calculated as well as the CVE of the delta band component $(0.5 - 4$ Hz). One thousand instances of simulated signals were used to obtain the average CVE, while the average spectral profile was obtained from 1000 instances of the summation of $2^{10} = 1024$ Poisson distributed pulses (similar results were generated with different numbers of pulses). Similarly, artificial signals were also generated by using as elementary events the following Alpha function (Rall, 1967) widely used to model synaptic conductance (g_{syn}). We adopted the equation from (De Schutter, 2010) ($g_{syn}(t) = \overline{g}_{syn} \cdot \frac{t-t_0}{\tau} \cdot e^{1-(t-t_0)/\tau}$), where $\overline{g}_{syn}$ is a scale factor determining the peak amplitude, t_0 is the event's starting time and τ is the time constant controlling the exponential decay. We simulate two conditions where λ_i ($\tau = 1/\lambda$) was uniformly distributed in the intervals $[0.1 - 100]$ s^{-1} and $[0.1 - 10]$ s^{-1}.

Bioethics statement. These experiments complied with American Physiological Society policies and were supervised by the Bioethics Committee of the *Facultad de Medicina* of the University of Chile.

Results

CVE for Gaussian noise. Before presenting our experimental data concerning the *CVE* of rat EEG, we must give some basic properties of the envelopes and their *CVE* for filtered white Gaussian noise (Fig. 1). Although it can be mathematically proven that the *CVE* for infinite Gaussian noise (as well as for any of its filtered sub-bands) is a constant equal to $\sqrt{\frac{4}{\pi} - 1} \approx 0.523$ (Schwartz et al., 1966), no closed-form result exists for discrete noise signals of arbitrary length. For example, 10 s segments of artificially constructed noise have individual *CVE* hovering near the 0.523 value (Fig. 1A); the same is true for its filtered bands (Fig. 1B and C). Thus, using computer simulation, we obtained the probability density distributions for *CVE* from filtered white Gaussian noise under different conditions of duration (5, 10, 20 and 40 s) and filter bandwidths (3, 6, 12 and 24 Hz). These probability density distributions for *CVE* are Gaussian-like, with a mode and a mean close to 0.523 and with a dispersion and skewness, depending on duration and bandwidth (Fig. 1D and E). As expected from analytical results, the *CVE* tends to

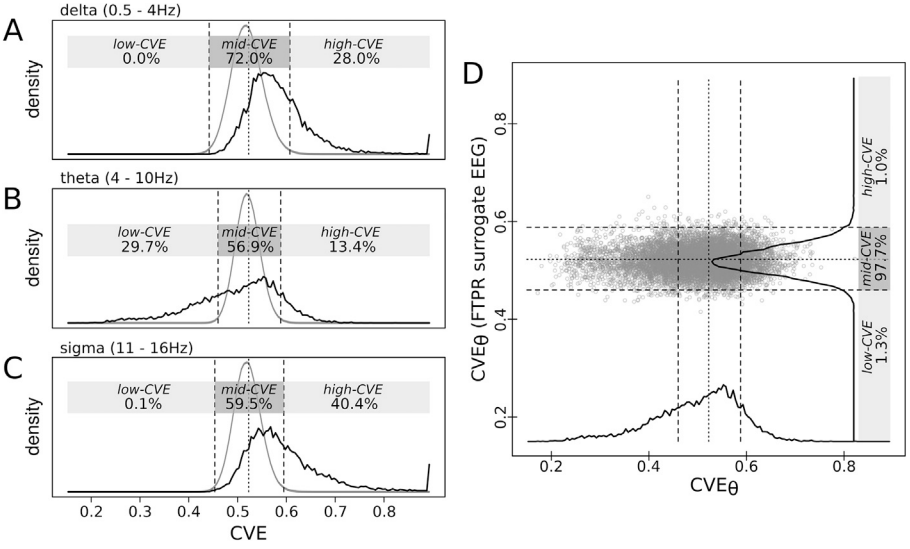

Fig. 2. *CVE* distributions for raw rat EEG and simulated data. (A) *CVE* distributions for 20 s epochs (50% overlap) of EEG delta band (CVE_δ) of a representative continuous 24 h period (black trace) totaling 8640 epochs, and from filtered Gaussian noise (grey trace) totaling 10^6 epochs. The same analysis for (B) theta and (C) sigma bands. For all panels the central dotted line shows the theoretical value of 0.523. Gaussianity confidence intervals (99%), for each case, are delimited by vertical dashes (delta: [0.442–0.607]; theta: [0.460–0.588]; sigma: [0.453–0.595]). These limits defined three intervals for the *CVE* range (*low-CVE*, *mid-CVE*, *high-CVE*). For experimental data, the frequency of occurrence inside the three *CVE* intervals is given by the corresponding percentages. CVE_θ is skewed towards low values, while CVE_δ and CVE_σ are skewed towards high values. (D) Scatter-plot between CVE_θ (x-axis) and CVE_θ for corresponding FTPR surrogate epochs (y-axis). Phase randomization collapses the broad and skewed empirical CVE_θ distribution (dark line in *X*-axis, same as in (B)) into a narrow and symmetrical distribution (dark line in *Y*-axis) containing 97.7% of its values inside the 99% confidence interval defined from theta filtered Gaussian noise (dashed lines).

narrower distributions, centered around 0.523 as the duration and bandwidth increase but as bandwidths, on the other hand becomes narrower the dispersion for *CVE* values increases while the mean and median departs significantly from 0.523. Thus, heavily filtered epoched signals should be avoided for CVE analysis.

Confidence intervals for CVE. As one of the aims of this work is to analyze how the classical delta, theta and sigma bands can be characterized by their *CVE*, we determined confidence intervals for testing the Gaussianity of observed EEG epochs. Taking into account the results shown in Fig. 1D, we chose for our analysis an epoch length of 20 s which provides good temporal resolution while avoiding large *CVE* variations inherent in small data samples. We calculated *CVE* distribution for 10^6 instances of 20 s intervals of Gaussian noise filtered in three bands of interest: 0.5 – 4 Hz (delta), 4 – 10 Hz (theta) and 11 – 16 Hz (sigma). From these distributions we obtained the 99% confidence intervals for the EEG Gaussianity hypothesis (H_0) for delta [0.442–0.607], theta [0.460–0.588] and sigma [0.453–0.595] respectively, defining three intervals: *low-CVE*, *mid-CVE*, and *high-CVE* (Fig. 2). Thus, for example, if a given epoch has a *CVE* inside the *mid-CVE* interval, we consider it to be, at the 99% level, indistinguishable from a Gaussian signal. The *CVE* probability density distributions for epochs from actual EEG bands (obtained from a 24 h EEG illustrative recording) share some properties with respect to their Gaussian model counterparts, such as their unimodal profiles and having their modes near the 0.523 value. *CVE* for delta (CVE_δ) and sigma (CVE_σ) bands show positive skewness and their *CVE* values are always in *mid-CVE* or *high-CVE* intervals. Interestingly *CVE* for theta (CVE_θ) band shows a negative skewness, exhibiting 29.7% of its values in the *low-CVE* interval and only 13.4% in the *high-CVE* interval (Fig. 2).

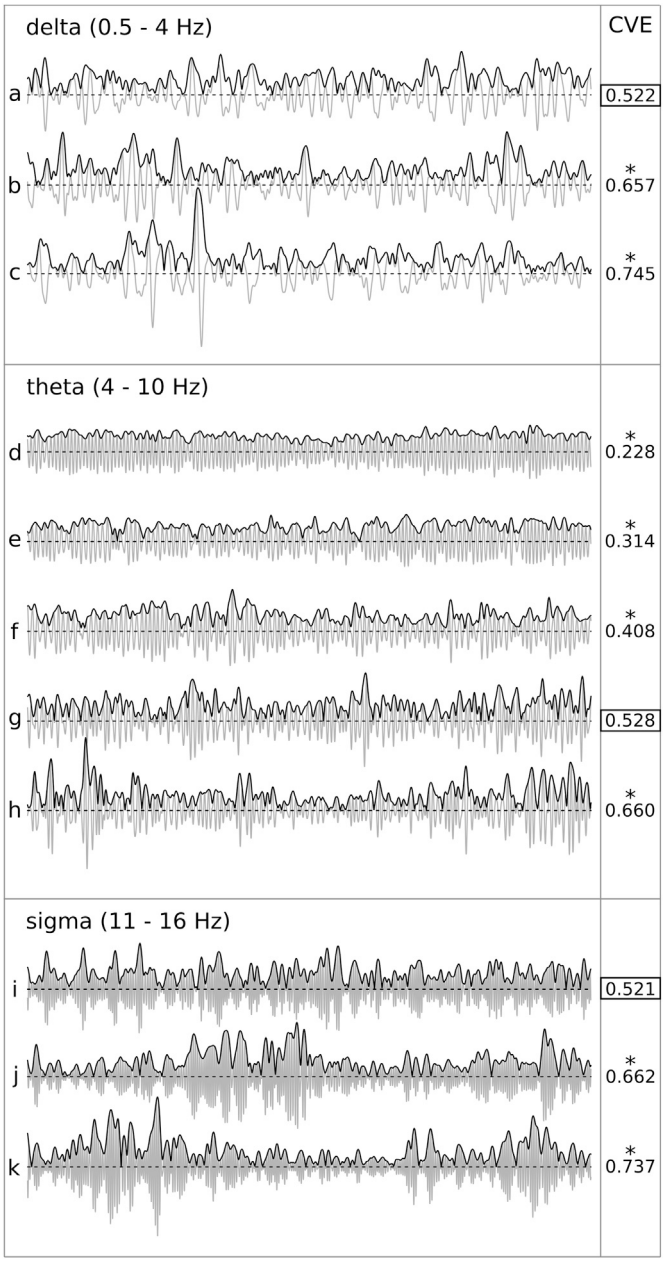

Fig. 3. Relationship between *CVE* and signal morphology. Eleven 20 s EEG segments (a-k) filtered in delta, theta and sigma bands are depicted (grey traces) with their respective envelopes (black traces) superimposed. The right column shows their associated *CVE*. Framed *CVE* values (a, g and i) indicate segments with *CVE* close to 0.523 while *CVE* values marked with '*' indicate segments outside *mid-CVE* interval. *CVE* values in the *low-CVE* interval correspond to epochs with very regular (i.e. quasi-sinusoidal) activity, revealing a rhythm only occurring in the theta band (d-f). *CVE* values in the *high-CVE* interval describe epochs with phasic activity (burst or spindle like profiles). Traces are scaled so that their mean amplitude is the same.

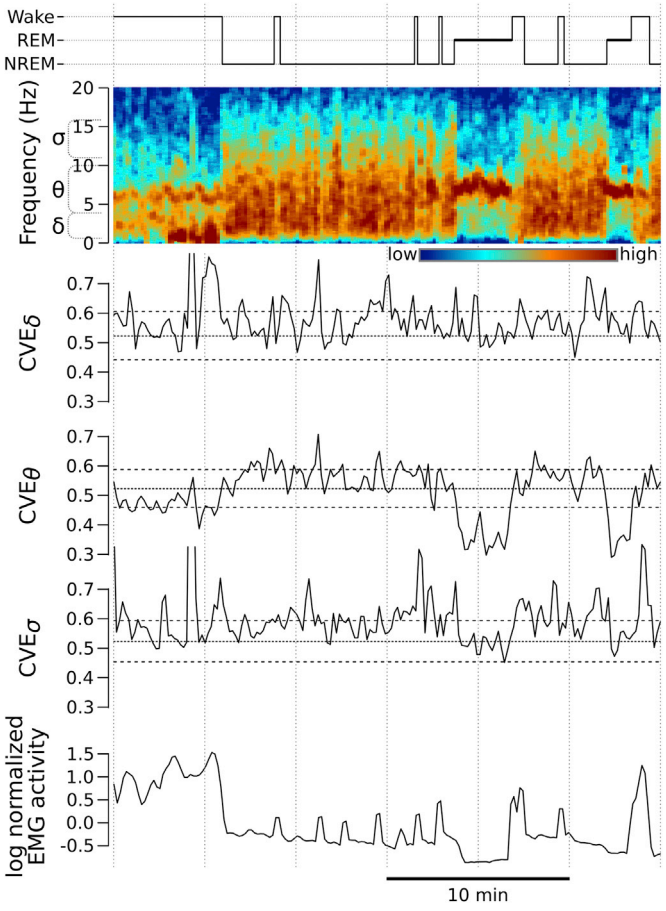

Fig. 4. Relations between sleep-wake states, EEG time-frequency representation, EMG and *CVE*. These six panels, from top to bottom: hypnogram, multitaper spectrogram, CVE_δ, CVE_θ, CVE_σ, and EMG show how these variables co-vary during a 0.5 h period exhibiting the three major behavioural states: wake, NREM and REM. REM sleep is clearly correlated with low CVE_θ and low EMG, while exhibiting a prominent theta peak (~ 7 Hz). NREM bouts have CVE_θ fluctuating in the *mid-CVE* and *high-CVE* intervals while exhibiting low EMG as well as a $1/f$ power spectrogram lacking clear localized peaks. Wake bouts have CVE_θ values straddling the boundary between *low-CVE* and *mid-CVE* while showing high EMG and a discernible, but variable, spectral theta power. For all *CVE* panels, central dotted line = 0.523, dashed lines = 99% confidence interval for the corresponding Gaussianity model.

We also explored the use of the FTPR surrogate data to test the suitability of our Gaussian model to determine the *mid-CVE* interval. As EEG spectral properties change dynamically it could be argued that FTPR epochs could better reflect the probabilistic model for EEG Gaussianity hypothesis (H_0). Thus, in the case of theta band, we calculated the distribution for a set of FTPR surrogates. Phase randomization produces a drastic change as the left-skewed distribution of CVE_θ is transformed into a distribution very similar to the one obtained by a filtered white Gaussian noise (Fig. 2D). While phase randomization maintains the epoch spectra, it destroys specific EEG phase relations and collapses its *CVE* into the *mid-CVE* interval. Similar results were obtained for delta and sigma bands (not shown). As the parameters describing the distributions for theta filtered white Gaussian noise *CVE* (1st Qu. = 0.504, median = 0.520, mean = 0.521, 3rd Qu. = 0.537, N = 1000000) and its Phase Randomization surrogate data (1st Qu. = 0.499, median = 0.518, mean = 0.519, 3rd Qu. = 0.538, N = 1002240) are very similar we used filtered white Gaussian noise as an operational model of Gaussianity for referential purposes.

The CVE of a signal reveals important morphological aspects of its temporal profile. From visual inspection it is possible to establish a relationship between the *CVE* value and the signal morphology of a given EEG epoch (Fig. 3). Epochs with *CVE* values near 0.523 appear like stationary filtered Gaussian noise (see traces *a, g* and *i*). *Low-CVE* epochs appear as rhythms having fairly sinusoidal profiles (see traces *d-f*). Note that the lower the *CVE* value, the more regular the theta rhythm (see the sequence *f*→*e*→*d*). On the other hand, *high-CVE* epochs reveal phasic or transient activity (see traces *b, c, h, j* and *k*). In general signals having envelopes with low dispersion with respect to their mean, like rhythms, have *low-CVE* (*d*) while pulsed signals (e.g. EEG spikes) are related to *high-CVE* values (*k*).

Relationships among CVE, spectrogram, EMG activity and behavioural states. CVE_θ correlates well with the animal's behavioural state (Fig. 4). During REM sleep, CVE_θ is mostly confined to the *low-CVE* interval. In this state, as is well known, the EEG spectrogram exhibits a prominent theta peak (~ 7 Hz). Also, EMG activity is at its lowest as REM is associated with muscular atony. During NREM sleep, CVE_θ straddles *mid-CVE* and *high-CVE* intervals and the corresponding spectrogram segment shows the well known $1/f$ profile (He et al., 2010), while the EMG also adopts low values. During the wake state, CVE_θ hovers near the *low-CVE* and *mid-CVE* interval boundary. The temporal courses of CVE_δ and CVE_σ greatly differ from CVE_θ as they seldom transit into *low-CVE* territory for any behavioral state.

Envelope characterization space. As *CVE* is a dimensionless (hence scale independent) metric, it is important to enquire how its values are correlated with the amplitude of the corresponding EEG band and behavioral states. Scatterplots between epoch band amplitudes (*y*-axis) and the corresponding *CVE* (*x*-axis), defining the *envelope characterization space*, show different clustering for delta, theta and sigma bands (Fig. 5,

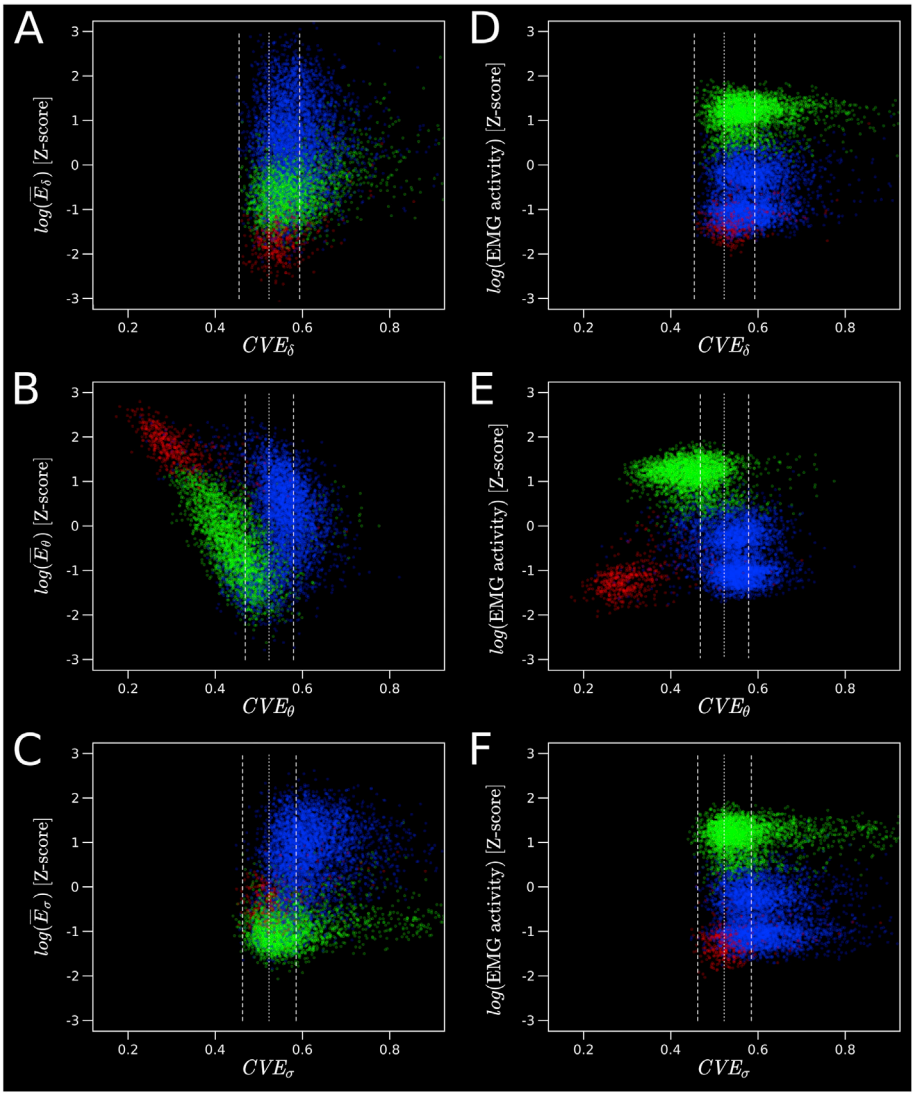

Fig. 5. Scatterplots of *EEG/EMG amplitude vs CVE* for delta, theta and sigma bands. *Left column*, Clusters representing the relation between *CVE* values and log-normalized EEG amplitude, for delta (A), theta (B), and sigma (C). Epochs are colored according to behavioral state (green = wake; blue = NREM; red = REM) and a 50% transparency (alpha channel = 0.5) was added to emphasize cluster density. For all three bands the low amplitude EEG is well centered in the *mid-CVE* (delimited by the dashed lines). As EEG amplitude increases, the three bands deviate from Gaussianity. For delta (A) and sigma (C) as EEG amplitude increases, the corresponding *CVE* values are confined to *mid-CVE* and *high-CVE* intervals. On the other hand, theta band (B) shows a clear v-shaped relationship. Large theta EEG amplitudes are located in the *low-CVE* interval (left branch of B, red dots corresponding to REM) or in the *mid-CVE* interval (vertical branch of B, blue dots corresponding to NREM). CVE_θ values located in the *high-CVE* interval are associated with epochs having intermediate theta EEG amplitudes. *Right column*, Clusters representing the relation between *CVE* values and log-normalized EMG amplitude, for delta (D), theta (E), and sigma (F). Theta band (E) shows well-defined and separated clusters correlated with behavioral states. Each dot represents a 20 s epoch, from an illustrative 24 h sleep-wake cycle, central dotted line = 0.523.

left column).

Scatterplots of CVE_δ vs. delta amplitude and CVE_σ vs. sigma amplitude reveal elongated clusters with *CVE* values in *mid-* and *high-CVE* intervals with clear segmentation by behavioral state along the *y*-axis for delta and sigma. In both cases the epochs with lowest amplitude correspond to epochs in the *mid-CVE* intervals and are fairly distributed around the 0.523 value. A relation exists between band amplitude and *CVE*: at high amplitude values there is a small, but consistent co-variation towards *high-CVE*. This correlation has the effect of producing right leaning clusters, constituted mainly by NREM (blue) epochs, and seems more marked for the sigma band.

The scatterplot of CVE_θ vs. theta amplitude shows a v-shaped relationship represented by a two-branched asymmetric cloud organized around the 0.523 value (Fig. 5B, left column). The left and upward pointing branch connects, with an almost linear relation, the small amplitude background activity with large regular sine-like waveforms involving mostly REM sleep (red) and wake states (green). Interestingly the apex of the branch contains REM sleep epochs almost exclusively and is made of epochs with the largest amplitudes and the lowest *CVE*. The vertical branch, which contains NREM sleep (blue) and wake states (green), shows that CVE_θ values are mostly contained in the *mid-CVE* interval, but with a small proportion straddling to the *high-CVE* interval especially at intermediate EEG theta amplitudes.

Scatterplots between EMG amplitude and *CVE* values are also informative. A clear clusterization is obtained in the case of theta band (Fig. 5E), as the data set divides itself into three well-separated clusters which correlate with behavioral states (B, right column). When using delta or sigma bands, these variables are unable to produce a similar clusterization (Fig. 5D,F). The cluster segmentation found in Fig. 5B and E opens the possibility of constructing new automatic EEG scoring algorithms using *CVE* as a relevant variable (which approximates the visual scoring rules that consider theta morphology).

The clear clusterization induced by EMG/ CVE_θ is a robust result. Fig. 6 shows 35 scatterplots of EMG-activity vs. CVE_θ, each corresponding to 24-h recordings from a data set constructed from seven rats (rats a-g) continuously recorded between 3 and 7 consecutive days. The three main clusters presented in Fig. 5E are also distinguishable in the 35 recording days analyzed. Importantly, the small cluster related to REM sleep is always well separated from the other clusters. The bottom-right inset shows the density map for the superposition of the complete data set, showing the same clusterization, where the REM associated cluster remains remarkably separated, pointing to a low inter-case variability.

Using density maps that superpose the complete data set over the envelope characterization space ($8640 \times 35 = 302400$ epochs), it is apparent that the clusterization is also robust (Fig. 7). The topological properties of the overall data set clusters match those of the illustrative case (compare clusters in 7A,B,C and Fig. 5A,B,C). In particular, the density map of the theta band is v-shaped (7B). Also, the *CVE* distributions of the complete data are fairly similar to those of the illustrative case of Fig. 2, indicating low variability between cases (compare distributions in 7A,B,C and Fig. 2A,B,C).

When the same data is plotted taking into consideration the EMG activity, an indicator of the animal behavioral state, the clusters show the segmentation already apparent in Fig. 5. For low EMG epochs, mostly corresponding to sleep epochs (NREM + REM), two clear clusters are revealed for theta (Fig. 7E). The smaller cluster has *low-CVE* values and large amplitudes while the large cluster has a large spread in amplitudes and its *CVE* values are mostly contained in the Gaussianity interval. This clear dichotomy (in accordance with the low overlap between red and blue clusters in 5B) is also clearly revealed by the bi-modal *CVE* distribution. For low EMG epochs, delta and sigma band density plots show a single elongated region containing two clusters (Fig. 7D,F). The minor cluster, confined to low amplitude epochs, is well centered in the *mid-CVE* range. The larger cluster contains a spread between large and medium size amplitudes, and its epochs are distributed in the *mid-* and *high-CVE* ranges forming a right skewed bulge (Fig. 7D,F).

For large EMG activity epochs, which correspond to active wake state, the theta band analysis shows an elongated left and upward pointing

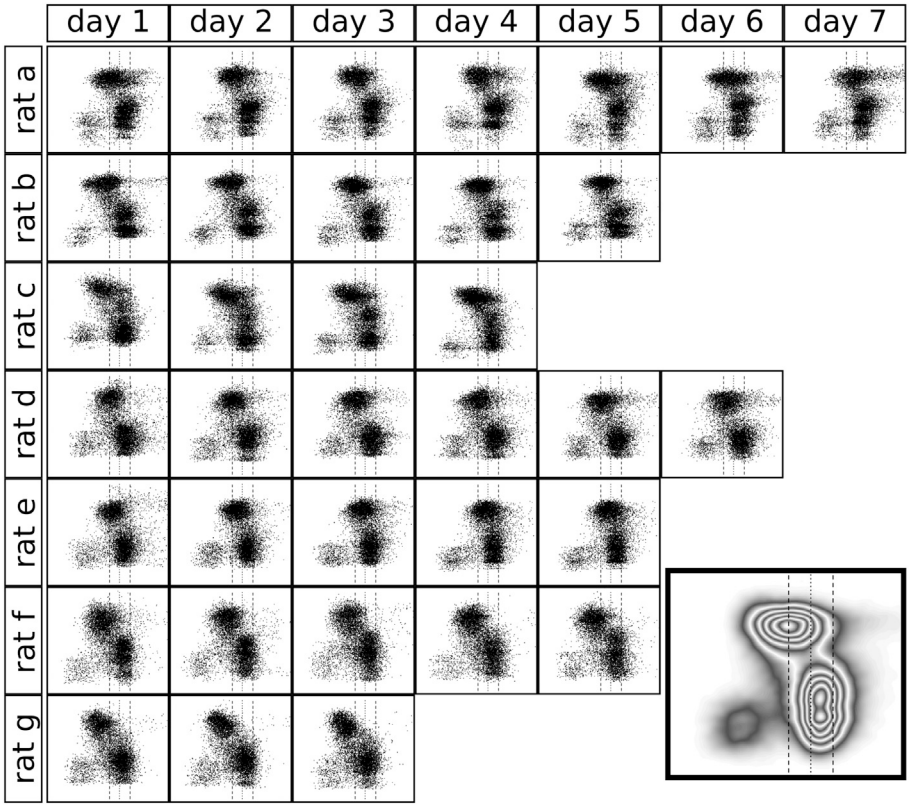

Fig. 6. Scatterplots between CVE_θ and EMG. The graph shows the scatterplots for our complete data set (35 recording days from 7 rats), generalizing Fig. 5 E, which corresponds to rat b, day 2. In all 35 sleep-wake cycles, three clusters appear. Bottom right inset corresponds to the 2D empirical density function for the 35 rats (colored in an alternating white-grey palette to provide a contour-plot-like style). In all panels the vertical lines mark the 0.523 value (dotted) and the theta *mid-CVE* interval (dashed).

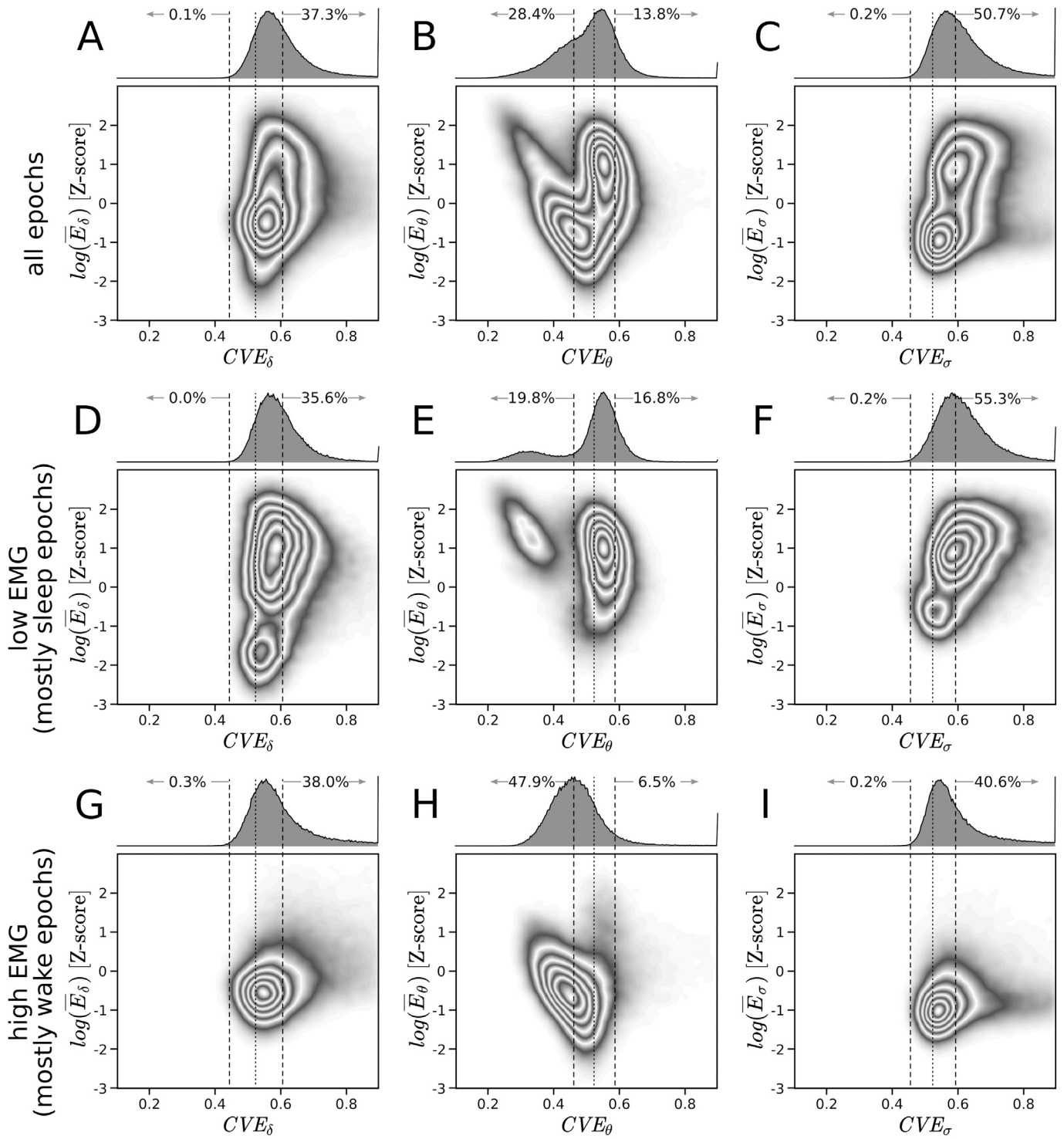

Fig. 7. Empirical density functions for EEG amplitude *vs CVE* values for delta, theta and sigma bands (35 days from 7 rats) **Upper-row (A-C)**, Density maps between *CVE* values and EEG amplitudes for all epochs ($8640 \times 35 = 302400$). The v-shaped relationship found for the single representative case in Fig. 5-B is clearly apparent across the complete data set (B). The empirical *CVE* distribution (top histogram in each panel) shows that CVE_θ is the only one with values denoting rhythmic activity (28.4% of epochs). Delta and sigma bands, as in Fig. 5-A,C, show a single, right-leaning cluster evidencing a positive correlation between EEG amplitude and *CVE*. **Middle-row (D-F)**, for low EMG epochs (1st tertile reflecting mostly NREM or REM states), the density maps for delta and sigma bands show the same clusters shifting to *high-CVE* values as amplitude increases, but for theta two clusters appeared, and they are associated with the bimodal distribution for CVE_θ. One cluster corresponds to epochs with large EEG amplitude but *low-CVE* (REM sleep). The more massive, central cluster has *CVE* values in the range of Gaussianity and large EEG amplitude. **Bottom-row (G-I)**, for epochs with large EMG activity (3rd-tertile reflecting mostly active wake) the distribution of *CVE* follows the same distribution for delta and sigma. CVE_θ distribution shows a Gaussian distribution, but straddling the boundary between *low-CVE* and *mid-CVE* intervals (H). Vertical dashed lines mark boundaries of *mid-CVE* interval while the dotted line indicates 0.523 value. The frequency of occurrence outside these intervals is given by the corresponding percentages. Density maps are colored in an alternating white-grey palette to provide a contour-plot-like style.

cluster that matches the green cluster of Fig. 5B. The distribution for CVE_θ straddles the boundary between *low/mid-CVE* intervals as almost half (47.9%) of *CVE* are in the *low-CVE* interval (Fig. 7H). In this condition delta and sigma bands produce single clusters centered near the critical value 0.523 and their *CVE* value distributions straddle the *mid/high-CVE* intervals (Fig. 7G,I). Finally, it is worth noting that for all analysis presented, *CVE* values corresponding to very low amplitude epochs are confined to the *mid-CVE* Gaussianity interval (Fig. 7 all panels).

To explain transient activity (phasic EEG) evidenced by *high-CVE*, we constructed a simple model in which EEG activity is assembled as the superposition of independent exponential decaying pulses of varying amplitude and with λ uniformly distributed in $[0.1 - 100]$ s^{-1}. We simulated artificial realizations by the poissonian superposition of $32, 64, \ldots, 8192$ pulses and calculated their *CVE* (Fig. 8). When the number of pulses is low, the signal has large *CVE* (Fig. 8A), low amplitude (Fig. 8B) and a temporal profile exhibiting clear pulses (Fig. 8 trace a). As the number of pulses increases, the temporal profiles become similar to filtered noise (Fig. 8 traces b and c), *CVE* asymptotically tends to the theoretical value of 0.523 (Fig. 8A) and the amplitude increases as $\sqrt{N}$

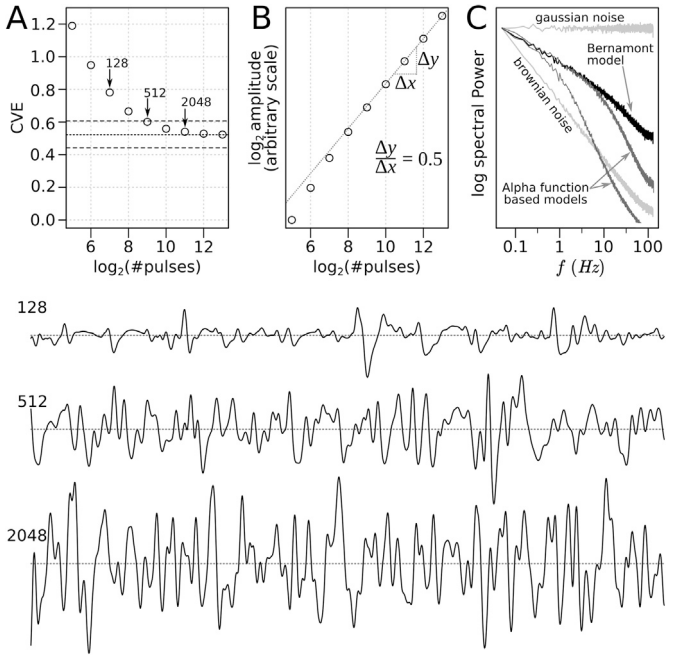

Fig. 8. *CVE* of artificial signals obtained by adding increasing numbers of Poisson distributed exponentialy decaying pulses. A. CVE_δ calculated for artificial signals constructed by adding different numbers of Poisson distributed pulses followed by delta filtering $(0.5 - 4$ Hz). Signals constructed with low number of pulses exhibit large CVE_δ that consistently diminish as the number of pulses increases. The *CVE* average asymptotically approaches the 0.523 value (dotted line). Dashed lines show the limits of *mid-CVE* interval for delta band. B. The average amplitude of the synthetic signals, as expected, increases with $\sqrt{pulses}$. Each data point is the average of 1000 instances of the simulation. C. Average spectra density for 100 simulated signals constructed by adding 1024 exponentialy decaying pulses of evenly distributed λ (Bernamont model, black trace) and similar computatinos using the alpha function (dark grey traces). These results aproximates scale-free processes with spectral profiles aproximatelly following the law $P \propto 1/f^\beta$. For the Bernamont model $\beta = 1$. For the alpha function based models β starts around 1 and bends to $\simeq 3$ where the "knee" location depends on λ distribution range (left trace $\lambda \sim [0.1 - 10]$; right trace $\lambda \sim [0.1 - 100]$). Gaussian noise ($\beta = 0$) and Brownian noise ($\beta = 2$) spectra (light grey traces) are also depicted as reference. All spectra share the value at the origin to facilitate comparison of their slopes. Bottom traces from top to bottom, illustrative instances of artificial signals produced with 128, 512, 2048 exponentially decaying pulses (traces are delta band filtered).

($N =$ number of pulses) as shown by the slope $= 0.5$ in a log-log plot (Fig. 8B). The average spectrum (1000 realizations) of the profiles obtained by adding 1024 exponentially decaying pulses produces a curve with an approximate average slope of -1 (Fig. 8C, black trace), corresponding to a numerical implementation of the classical model explaining the $1/f$ spectrum associated to flicker-noise in vacuum tubes (Bernamont, 1937). Gaussian and Brownian noises with slopes of 0 and -2 respectively were also calculated as reference (Fig. 8C, light grey traces). We further investigated the superposition of pulses based on the alpha function, a widely used model of synaptic conductance (Rall, 1967). In this case we obtained interesting features (Fig. 8C, dark grey traces) observed in real EEG, like "knees" and slopes higher than 2 in log-log spectra (He, 2014). The "knee" location can be controlled adjusting the distribution of λ values (see methods).

Discussion

CVE as a measure of gaussianity and signal morphology

Signal envelopes, commonly used in science/engineering, have been used in neuroscience to describe EEG amplitudes (Clochon et al., 1996; Freeman, 2004; Tao and Mathur, 2010) and here we focus on the *CVE* as a scale-independent descriptor of signal morphology and Gaussianity (Díaz et al., 2007, 2014). Recently Cole and Voytek underlined the importance of waveform shape of brain oscillations, in particular, their non-sinusoidal aspects which are difficult to characterize with Fourier techniques (Cole and Voytek, 2017) while others have stressed the importance of developing metrics to define "rhythmic" or "sinusoidal" processes, as even noise could produces sinusoidal-like activity when undergoing filtering (Jones, 2016; Cohen, 2017) (Fig. 1).

Our approach, based on well-known properties of white Gaussian noise and narrow band noise (Schwartz et al., 1966), assesses EEG Gaussianity using *CVE* as a metric and constructs, for each band, three confidence intervals which correlate with signal morphology (Fig. 3). Altough CVE_δ, CVE_θ and CVE_σ exhibit deviations from Gaussianity, only CVE_θ straddles into its corresponding *low-CVE* interval while CVE_δ and CVE_σ only span their *mid* and *high-CVE* intervals. Using FTPR we showed that any deviation in the estimation of Gaussianity due to particular spectral properties at the epoch level is minimal (Fig. 2D). Thus, our Gaussianity model based on filtered white Gaussian noise can be considered a fair model for Gaussianity in EEG studies. On the other hand FTPR shows (as FTPR destroy phase relationships, while maintaining the spectral properties) that some special envelope features like rhythms and phasic activity (Fig. 3), are produced by EEG specific phase configurations which can not be only characterized using spectral analysis.

Overall, *CVE* defines an scale pointing to relevant aspects of signal morphology and with this scale, qualitative categorizations (for example the widely-used hippocampal LFP types, such as theta rhythm, large-amplitude irregular activity, and small-amplitude irregular activity (Vanderwolf, 1969; Bland, 1986; Jarosiewicz et al., 2002) may be now quantitatively reassessed. Moreover, epoch-based *CVE* analysis provides a practical description of neural dynamics as *CVE* fluctuations are correlated with animal behavioural states (Fig. 4).

Envelope characterization space

EEG is a wave phenomenon originating from the linear superposition of a massive number of neuronal current sources distributed across many anatomical scales and functional types, showing significant changes in amplitude and morphology during the sleep-wake cycle. According to the central limit theorem, if those sources were uncorrelated, EEG signals should have properties of a Gaussian process (Elul, 1969; McEwen and Anderson, 1975; Gonen and Tcheslavski, 2012). Instead, if a significant amount of sources were correlated (i.e. neural synchrony), EEG should deviate from Gaussianity as correlation/synchrony produces constructive interference, increasing signal amplitude. The *envelope characterization*

space (Figs. 5 and 7) shows a novel synthesis of EEG dynamics exhibiting deviations from Gaussianity correlated with EEG amplitude, indicating that for some time periods, something other than the mere interference of uncorrelated waves is occurring. We propose that these deviations to *low-CVE* and to *high-CVE* correspond to two conceptually different manifestations of neural synchrony.

In the case of deviations to *low-CVE*, the link to neural synchrony is straightforward. Epochs showing *low-CVE* are related to theta rhythm, considered "the largest extracellular synchronous signal that can be recorded from the mammalian brain" (Vertes, 2005). The left up-pointing densities (Figs. 5B and 7B, E) in the envelope characterization space show a correlation between *low-CVE* and signal amplitude that clearly indicate how theta rhythm becomes more coherent while augmenting its amplitude, strongly suggesting an underlying neural synchronization process. Indeed, this correlation matches the behaviour of the well-studied Kuramoto model, where weakly coupled oscillators pull each other to a common frequency producing a collective oscillation of increasing amplitude as constructive interference dominates the system (Strogatz, 2000; Díaz et al., 2007; Breakspear et al., 2010; Schmidt et al., 2015).

On the other hand, epochs deviating from Gaussianity towards *high-CVE*, mostly found in NREM sleep, show a peculiar combination of features — high amplitude gaussian waves (delta waves) coexisting with phasic activity and a high-power $1/f$ spectral profile lacking a prominent peak (Fig. 4). As suggested by the phasic activity reported by *CVE*, pointing to pulses over EEG background, we propose a model that recreates the properties of EEG concerning its envelope morphology during NREM sleep. In this state EEG is interpreted as the superposition of Poisson-distributed (i.e. arrhythmic) transient waveforms appearing at different temporal rates (Fig. 8). For a small number of events, the *CVE* adopts rather large values while the EEG amplitude remains low. As the number of independent events increases, *CVE* decreases and converges to 0.523, while the overall simulated signal gains amplitude $\propto\sqrt{N}$ (*N*: number of transients) as expected for out-of-phase wave superposition (Elul, 1971; Díaz et al., 2007) (Fig. 8A and B). Thus, the coexistence of high-amplitude gaussian waves and phasic activity (transitions between *mid-* and *high-CVE*) can be explained just by varying the transients' rate. Interestingly, human NREM sleep is characterized by a progressive increase in the apparent delta band density as the subject reaches deeper NREM sleep stages, going from K-complexes, to delta phasic activity, to delta waves (Terzano et al., 1985; Halasz and Bódizs, 2013).

Our model also illuminates the origin of EEG's $1/f$ spectral signature (Ward, 2002; He et al., 2010). As a first approximation, the simulated events were implemented as *exponentially decaying functions*, recreating the classic framework explaining the origin of flicker noise (i.e. $1/f$ noise) in vacuum tubes (Bernamont, 1937; Milotti, 2002). In this condition the resulting simulated signals have a $1/f$ spectral signature (Fig. 8C). Exponentially decaying functions are relevant for EEG properties, since post-synaptic potentials, pointed out as being the main contributors of extracellular field potentials (Buzsáki et al., 2012), are characterized by sharp deflections followed by slower exponential decays. Sharp-edged waveforms have broadband spectral signatures unrelated to rhythmic activity (Kramer et al., 2008; Ray and Maunsell, 2011), while the spectral properties of exponentially decaying functions are probably responsible for the EEG $1/f$ profile (Miller et al., 2009). In addition, we also considered a more realistic model of synaptic conductance (alpha function) where the rising phase is not infinitely fast (De Schutter, 2010). In this condition, spectral profiles closer to reality are obtained (Fig. 8C dark grey traces) as the phenomenon colloquially referred as $1/f$ spectrum in the brain context, corresponds to a $1/f^{\beta}$ law with $0 < \beta < 4$ and is not strictly linear either (He et al., 2010). The EEG spectrum profile shaped by the palette of time constants related to membrane potentials is consistent with general anesthetics' altering those time constants at multiple targets (Bai et al., 1999; Li and Pearce, 2000; Pittson et al., 2004; Hemmings et al., 2005; Franks, 2008) making EEG spectrum more tilted to low frequencies and reducing the apparent spectral edge (Purdon et al., 2013).

Certainly, to properly model the effect of synaptic activity in EEG profiles requires considering the non-trivial relationships between neuronal currents and the extracellular electrical field potentials (Hales and Pockett, 2015). Nevertheless, empirical data show that exponential-like transients are commonly recognized in neuronal recordings at the meso-scale level (see Fig. 3 in Luczak et al., 2015 and Fig. 1 in Plenz and Thiagarajan, 2007). Recently, new kinds of neuronal correlated activity have been recognized, characterized by neural transient events or *activity packets* which are manifested in multi-unit activity recordings as neuronal population spiking concentrated in discrete time windows and in LFP recordings as transient voltage deflections (e.g. hippocampal sharp waves, negative LFPs in cortical avalanches, etc) (Luczak et al., 2015). This ubiquitous phenomena, observed in many brain areas of multiple species, are thought to represent the basic building blocks of cortical coding (Luczak et al., 2015) and their time intervals appear irregular (Plenz and Thiagarajan, 2007) or Poisson distributed (Buzsáki, 2015). Thus, concurrent post-synaptic potentials triggered during *activity packets* could produce the transients required in our model. This simultaneous neural activity corresponds to the fundamental type of neural synchrony originating *neural assemblies*, that can be simply defined as the temporal proximity enabling superposition in the extracellular field (Plenz and Thiagarajan, 2007).

Concluding remarks

The envelope characterization space (i.e. $log(\overline{E})$ vs. *CVE*) introduced here reveals remarkable relations showing special constraint between EEG's amplitude and morphology that suggests a new framework for EEG interpretation. First, our envelope analysis shows that low amplitude EEG background noise appears Gaussian for delta, theta and sigma bands. Second, and more crucially, two modes for departing from Gaussianity are revealed and both are associated with large EEG amplitudes (Fig. 9). As previously predicted for synchronous waves (Díaz et al., 2007), theta rhythm showed a correlation between *low-CVE* and large amplitudes (Fig. 9 a,b) while the regime characterized by deviations from Gaussianty towards *high-CVE* can be explained by the arrhythmic superposition of EEG transients (Fig. 9 c_1,c_2). The temporal profile of these transients is usually close to exponentially decaying functions whose spectral properties can explain the colored EEG spectrum. Conceiving EEG as mainly originated by the superposition of neural *activity packets* producing transients of many sizes (recruiting neural masses of different sizes), it is possible to explain why $1/f$ spectra are present from background EEG to high-amplitude EEG and observed in all behavioral states, while rhythmic activity —due to the synchronization of weakly coupled oscillators— only occurs episodically as spectral peaks over a $1/f$ background (He, 2014). This interpretation is consistent with experimental results showing that neuronal avalanches during NREM sleep are larger than in other behavioural states (Priesemann et al., 2013).

The model presented serves to link phenomena like the broadband scale-free activity with irregular processes like neuronal avalanches. This link is important as it has been suggested that such a unifying framework should be an important step in EEG research (He, 2014). *CVE* analysis places deviations from Gaussianity, synchrony and the origin of the $1/f$ spectra in the same domain. At the same time it obligates a closer consideration of the definition of neural synchrony. In effect, in our model, two types of synchronization dynamics are required to explain divergent properties in EEG's time and frequency domains. Rhythmic waves, on one hand, exhibit the dynamical properties of a *synchronization of weakly coupled oscillators* (Lubenov and Siapas, 2009; Goutagny et al., 2009) while, on the other hand, EEG transients represent *concurrent neuronal activity*, a broader interpretation of synchrony, associated to the very definition of neural assemblies (Buzsáki, 2010; Plenz and Thiagarajan, 2007; Hebb, 1949).

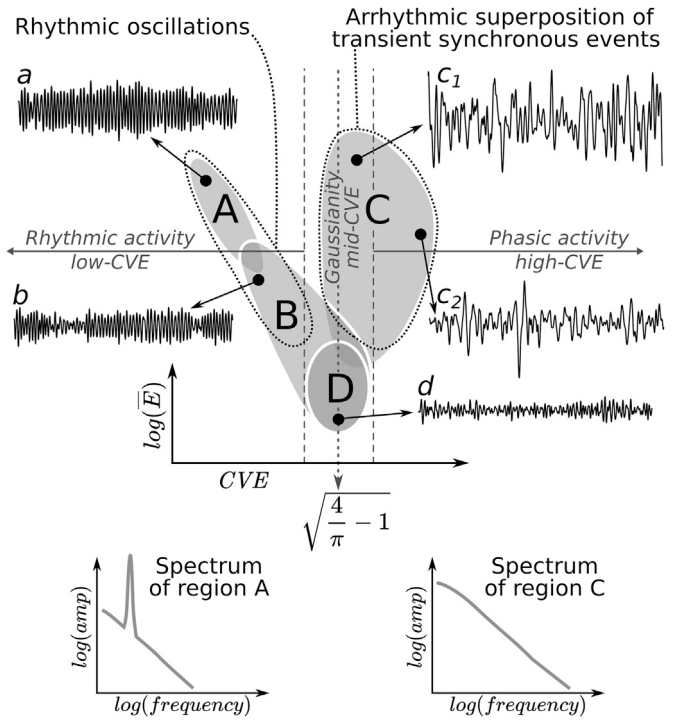

Fig. 9. *Envelope characterization space* analysis: summary of main results. Projecting epochs of rat EEG sleep cycle into the $log(\overline{E})$ *vs CVE* characterization space produces an asymmetric clustering, organized around the $CVE = \sqrt{4/\pi - 1} \approx 0.523$ axis, that can be subdivided into regions correlated with behavioural states. Regions A, B (which appear only for theta band) are visible during REM sleep and wake respectively (Fig. 5B, 7E and 7H). Region C, which is visible for all studied bands but is more prominent for delta and sigma during NREM sleep (Fig. 5A, C, 7D and 7F). Region D appears in the lower amplitude range of all EEG bands and represents EEG background activity (Fig. 5 and 7). Real traces *a-d* illustrates EEG signal morphology related to the different regions (traces *a, b* and *d*: theta band; traces c_1 and c_2: delta band). These morphologies can be categorized into rhythmic (*low-CVE*), Gaussian (*mid-CVE*) or phasic (*high-CVE*). Dotted and dashed lines indicate $CVE = 0.523$ and the lower and upper boundaries of the *mid-CVE* interval respectively. Bottom insets illustrate the spectral properties of epochs belonging to regions A (prominent peak in theta band) and C ($1/f$ profile) as illustrated in Fig. 4. Thus, from Gaussian background EEG (region D) two routes to high EEG amplitudes are possible (enclosed in dark dotted lines). One route leads to the appearance of rhythmic oscillations (*a*, *b*), associated to *low-CVE*. The second route emerges from the arrhythmic superposition of transient synchronous events, producing Gaussian waves (c_1) and phasic patterns (c_2), associated to *mid-* and *high-CVE*

Acknowledgments

We thank Jorge Estrada for surgical procedures and Diane Greenstein for editorial assistance. Also we want to thank the reviewers for their valuable suggestions. This research was supported in part by Fundación Puelma (Facultad de Medicina, Universidad de Chile) and FONDECYT grants 1060250, 1061089.

References

Adrian, E.D., Matthews, B.H.C., 1934. The berger rhythm: potential changes from the occipital lobes in man. Brain 57, 355–385.
Bai, D., Pennefather, P.S., MacDonald, J.F., Orser, B.A., 1999. The general anesthetic propofol slows deactivation and desensitization of gaba(a) receptors. J. Neurosci. 19, 10635–10646.
Beggs, J.M., Plenz, D., 2004. Neuronal avalanches are diverse and precise activity patterns that are stable for many hours in cortical slice cultures. J. Neurosci. 24, 5216–5229.
Bernamont, J., 1937. Fluctuations de potential aux bornes d'un conducteur metallique de faible volume parcouru par un courant. Ann. Phys. 79, 71–140.
Bland, B.H., 1986. The physiology and pharmacology of hippocampal formation theta rhythms. Prog Neurobiol 26, 1–54.
Breakspear, M., Heitmann, S., Daffertshofer, A., 2010. Generative models of cortical oscillations: neurobiological implications of the kuramoto model. Front. Hum. Neurosci. 4, 190.
Buzsáki, G., 2010. Neural syntax: cell assemblies, synapsembles, and readers. Neuron 68, 362–385.
Buzsáki, G., 2015. Hippocampal sharp wave-ripple: a cognitive biomarker for episodic memory and planning. Hippocampus 25, 1073–1188.
Buzsáki, G., Anastassiou, C.A., Koch, C., 2012. The origin of extracellular fields and currents — eeg, ecog, lfp and spikes. Nat. Rev. Neurosci. 13, 407–420.
Castro-Faúndez, J., Díaz, J., Ocampo-Garcés, A., 2016. Temporal organization of the sleep-wake cycle under food entrainment in the rat. Sleep 39, 1451–1465.
Clochon, P., Fontbonne, J., Lebrun, N., Etévenon, P., 1996. A new method for quantifying eeg event-related desynchronization:amplitude envelope analysis. Electroencephalogr. Clin. Neurophysiol. 98, 126–129.
Cohen, M.X., 2017. Where does eeg come from and what does it mean? Trends Neurosci. 40, 208–218.
Cole, S.R., Voytek, B., 2017. Brain oscillations and the importance of waveform shape. Trends Cognit. Sci. 21, 137–149.
Díaz, J., Razeto-Barry, P., Letelier, J.C., Caprio, J., Bacigalupo, J., 2007. Amplitude modulation patterns of local field potentials reveal asynchronous neuronal populations. J. Neurosci. 27, 9238–9245.
Díaz, J.A., Arancibia, J.M., Bassi, A., Vivaldi, E.A., 2014. Envelope analysis of the airflow signal to improve polysomnographic assessment of sleep disordered breathing. Sleep 37, 199–208.
De Schutter, E., 2010. Computational Modeling Methods for Neuroscientists. MIT Press, Cambridge, MA.
Elul, R., 1969. Gaussian behavior of the electroencephalogram: changes during performance of mental task. Science 164, 328–331.
Elul, R., 1971. The genesis of the eeg. Int. Rev. Neurobiol. 15, 227–272.
Franks, N.P., 2008. General anaesthesia: from molecular targets to neuronal pathways of sleep and arousal. Nat. Rev. Neurosci. 9, 370–386.
Freeman, W.J., 2004. Origin, structure, and role of background eeg activity. part 1. analytic amplitude. Clin. Neurophysiol. 115, 2077–2088.
Freeman, W.J., 2006. Origin, structure, and role of background eeg activity. part 4: neural frame simulation. Clin. Neurophysiol. 117, 572–589.
Galka, A., 2000. Topics in Nonlinear Time Series Analysis: with Implications for EEG Analysis. World Scientific, London.
Gonen, F.F., Tcheslavski, G.V., 2012. Techniques to assess stationarity and gaussianity of eeg: an overview. Int J BIOautomation 16, 135–142.
Goutagny, R., Jackson, J., Williams, S., 2009. Self-generated theta oscillations in the hippocampus. Nat. Neurosci. 12, 1491–1493.
Halasz, P., Bódizs, R., 2013. Dynamic Structure of NREM Sleep. Springer, London.
Hales, C.G., Pockett, S., 2015. The relationship between local field potentials (lfps) and the electromagnetic fields that give rise to them. Front. Syst. Neurosci. 8, 233.
Harris, K.D., Thiele, A., 2011. Cortical state and attention. Nat. Rev. Neurosci. 12, 509–523.
He, B.J., 2014. Scale-free brain activity: past, present, and future. Trends Cognit. Sci. 18, 480–487.
He, B.J., Zempel, J.M., Snyder, A.Z., Raichle, M.E., 2010. The temporal structures and functional significance of scale-free brain activity. Neuron 66, 353–369.
Hebb, D.O., 1949. The Organization of Behavior. Wiley, New York, NY.
Hemmings, H.C., Akabas, M.H., Goldstein, P.A., Trudell, J.R., Orser, B.A., Harrison, N.L., 2005. Emerging molecular mechanisms of general anesthetic action. Trends Pharmacol. Sci. 26, 503–510.
Jarosiewicz, B., McNaughton, B.L., Skaggs, W.E., 2002. Hippocampal population activity during the small-amplitude irregular activity state in the rat. J. Neurosci. 22, 1373–1384.
Jones, S.R., 2016. When brain rhythms aren't 'rhythmic': implication for their mechanisms and meaning. Curr. Opin. Neurobiol. 40, 72–80.
Kramer, M.A., Tort, A.B., Kopell, N.J., 2008. Sharp edge artifacts and spurious coupling in eeg frequency comodulation measures. J. Neurosci. Meth. 170, 352–357.
Li, X., Pearce, R.A., 2000. Effects of halothane on gaba(a) receptor kinetics: evidence for slowed agonist unbinding. J. Neurosci. 20, 899–907.
Linkenkaer-Hansen, K., Nikouline, V.V., Palva, J.M., Ilmoniemi, R.J., 2001. Long-range temporal correlations and scaling behavior in human brain oscillations. J. Neurosci. 21, 1370–1377.
Lubenov, E.V., Siapas, A.G., 2009. Hippocampal theta oscillations are travelling waves. Nature 459, 534–539.
Luczak, A., McNaughton, B.L., Harris, K.D., 2015. Packet-based communication in the cortex. Nat. Rev. Neurosci. 16, 745–755.
Matthews, P.C., Mirollo, R.E., Strogatz, S.H., 1991. Dynamics of a large system of coupled nonlinear oscillators. Physica D 52, 293–331.
McEwen, J.A., Anderson, G.B., 1975. Modeling the stationarity and gaussianity of spontaneous electroencephalographic activity. IEEE Trans. Biomed. Eng. 22, 361–369.
Miller, K.J., Sorensen, L.B., Ojemann, J.G., den Nijs, M., 2009. Power-law scaling in the brain surface electric potential. PLoS Comput. Biol. 5, e1000609.
Milotti, E., 2002. A Pedagogical Review of 1/f Noise. ArXiv: Physics/0204033.
Motokawa, K., Mita, T., 1942. Das wahrscheinlichkeitsprinzip über die gehirnelektrischen erscheinungen des menschen. Jap J med Sci Biophys 8, 63–77.
Nunez, P.L., Srinivasan, R., 2006. Electric Fields of the Brain: the Neurophysics of EEG. Oxford University Press, New York, NY.

Pittson, S., Himmel, A.M., MacIver, M.B., 2004. Multiple synaptic and membrane sites of anesthetic action in the ca1 region of rat hippocampal slices. BMC Neurosci. 5, 52.
Plenz, D., Thiagarajan, T.C., 2007. The organizing principles of neuronal avalanches: cell assemblies in the cortex? Trends Neurosci. 30, 101–110.
Prerau, M.J., Brown, R.E., Bianchi, M.T., Ellenbogen, J.M., Purdon, P.L., 2016. Sleep neurophysiological dynamics through the lens of multitaper spectral analysis. Physiology 32, 60–92.
Priesemann, V., Valderrama, M., Wibral, M., Le Van Quyen, M., 2013. Neuronal avalanches differ from wakefulness to deep sleep–evidence from intracranial depth recordings in humans. PLoS Comput. Biol. 9, e1002985.
Purdon, P.L., Pierce, E.T., Mukamel, E.A., Prerau, M.J., Walsh, J.L., Wong, K.F., Salazar-Gomez, A.F., Harrell, P.G., Sampson, A.L., Cimenser, A., Ching, S., Kopell, N.J., Tavares-Stoeckel, C., Habeeb, K., Merhar, R., Brown, E.N., 2013. Electroencephalogram signatures of loss and recovery of consciousness from propofol. Proc. Natl. Acad. Sci. U. S. A. 110, E1142–E1151.
Rall, W., 1967. Distinguishing theoretical synaptic potentials computed for different soma-dendritic distributions of synaptic input. J. Neurophysiol. 30, 1138–1168.
Rao, R., Edwards, E., 2008. F1000prime recommendation of Díaz J et al. J. Neurosci. 2007 27 (34), 9238–9245. F1000Prime.com/1127024.
Ray, S., Maunsell, J.H., 2011. Different origins of gamma rhythm and high-gamma activity in macaque visual cortex. PLoS Biol. 9, e1000610.
Robert, C., Guilpin, C., Limoge, A., 1999. Automated sleep staging systems in rats. J. Neurosci. Meth. 88, 111–122.
Sato, K., 1957. An interpretation concerning physiological significance of statistical nature of electroencephalogram. Folia Psychiatr. Neurol. Jpn. 10, 283–294.
Saunders, M.G., 1963. Amplitude probability density studies on alpha and alpha-like patterns. Electroencephalogr. Clin. Neurophysiol. 15, 761–767.
Schmidt, R., LaFleur, K.J., de Reus, M.A., van den Berg, L.H., van den Heuvel, M.P., 2015. Kuramoto model simulation of neural hubs and dynamic synchrony in the human cerebral connectome. BMC Neurosci. 16, 54.
Schwartz, M., Bennett, W.R., Stein, S., 1966. Communication Systems and Techniques. McGraw-Hill, New York, NY.
Singer, W., Gray, C.M., 1995. Visual feature integration and the temporal correlation hypothesis. Annu. Rev. Neurosci. 18, 555–586.
Steriade, M., Datta, S., Paré, D., Oakson, G., Curró Dossi, R.C., 1990. Neuronal activities in brain-stem cholinergic nuclei related to tonic activation processes in thalamocortical systems. J. Neurosci. 10, 2541–2559.
Stern, J.M., Engel, J., 2005. Atlas of EEG Patterns. LWW, Philadelphia, PA.
Strogatz, S.H., 2000. From kuramoto to crawford: exploring the onset of synchronization in populations of coupled oscillators. Physica D 143, 1–20.
Tao, J.D., Mathur, A.M., 2010. Using amplitude-integrated eeg in neonatal intensive care. J. Perinatol. 30, S73–S81.
Terzano, M.G., Mancia, D., Salati, M.R., Costani, G., Decembrino, A., Parrino, L., 1985. The cyclic alternating pattern as a physiologic component of normal nrem sleep. Sleep 8, 137–145.
Vanderwolf, C.H., 1969. Hippocampal electrical activity and voluntary movement in the rat. Electroencephalogr. Clin. Neurophysiol. 26, 407–418.
Varela, F., Lachaux, J.P., Rodriguez, E., Martinerie, J., 2001. The brainweb: phase synchronization and large-scale integration. Nat. Rev. Neurosci. 2, 229–239.
Vertes, R.P., 2005. Hippocampal theta rhythm: a tag for short-term memory. Hippocampus 15, 923–935.
von der Malsburg, C., 2000. The what and why of binding: the modeler's perspective. Neuron 24, 95–104, 111.
Ward, L.M., 2002. Dynamical Cognitive Science. MIT Press, Cambridge, MA.